Synthesis, structural and in-vitro functional studies of half-sandwich platinum group metal complexes having various bonding modes of benzhydrazone derivative ligands

Lathewdeipor Shadap[a], Jaya Lakshmi Tyagi[b], Krishna Mohan Poluri[b], Emma Pinder[c], Roger M. Phillips[c], Werner Kaminsky[d], Mohan Rao Kollipara[a*]

[a]Centre for Advanced Studies in Chemistry, North-Eastern Hill University, Shillong 793 022, India. E-mail: mohanrao59@gmail.com

[b]Department of Biotechnology and Centre for Nanotechnology, Indian Institute of Technology Roorkee, Roorkee- 247 667, India.

[c]Department of Pharmacy, School of Applied Sciences, University of Huddersfield, Queensgate, Huddersfield, HD1 3DH, UK

[d]Department of Chemistry, University of Washington, Seattle, WA 98195, USA

Graphical abstract

Benzhydrazone half-sandwich platinum group metal complexes were prepared by the reaction of metal precursors and benzhydrazone derivative ligands which yielded chelating N∩O and N∩N bidentate cationic complexes. Ruthenium complexes formed N∩O while rhodium and iridium complexes formed N∩N bonding modes respectively. Antibacterial activity (against Gram-positive and Gram-negative bacteria) as well as anti-cancer (HCT116 $p53^{+/+}$ and HCT116 $p53^{-/-}$) studies for these complexes were carried out.

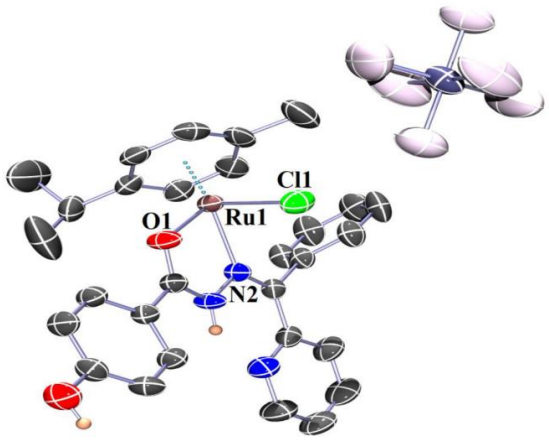

Complex 4

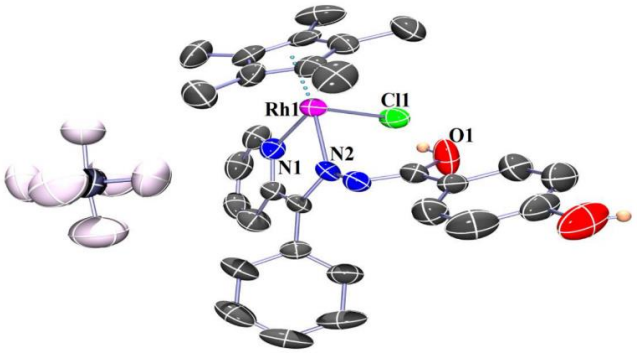

Complex 5

Abstract

Complexes **1-9** were synthesized by reacting metal precursors $[(arene)MCl_2]_2$ (arene = *p*-cymene, Cp*; M = Ru, Rh and Ir) and benzhydrazone derivative ligands **L1**, **L2** and **L3** which resulted in the formation of cationic complexes with PF_6 as the counter ion. Ruthenium complexes exhibited N∩O bonding mode while rhodium and iridium complexes exhibited N∩N bonding mode with the migration of the N-H proton to the adjacent C=O (keto) group forming enol. Anti-bacterial activity studies (against Gram-positive and Gram-negative bacteria) as well as anti-cancer [HCT116 p53 wild type ($p53^{+/+}$) and HCT116 p53 null ($p53^{-/-}$)] were carried out for all the complexes as well as ligands where interestingly, ligand **L2** and complex **5** showed high activity potency (*in-vitro)* for both biological studies. Amongst Ru, Rh and Ir, rhodium complexes showed more anticancer activity.

Keywords: Ruthenium, rhodium, iridium, benzhydrazone, *in-vitro* studies

Introduction

Much attention has been paid to platinum group metal complexes because of their distinctive properties such as the ability to form stable complexes where π-ligated arene provides great stability to the metal centre thereby influencing their hydrophobicity and interaction with biomolecules [1]. Platinum group metals like ruthenium, rhodium and iridium have been reported to exhibit many properties like catalytic, photochemical and biological activities [2, 3]. The effect of metal-based drugs depends not only on the properties of the metal but also on ligand moieties. To investigate the properties of metal complexes whether catalytically or biologically, ligand modification is a common route. In this study, we have synthesized half-sandwich metal complexes of ruthenium, rhodium and iridium containing benzoyl pyridine-benzhydrazone derivative ligands. The ligands (Chart 1) have been prepared according to the reported procedures [4-7]. Hydrazone derivatives are an important class of ligands with interesting ligation properties and the hydrazone unit offers a degree of rigidity, a conjugated π-system and a N-H unit which may participate in hydrogen bonding and may undergo protonation–deprotonation [8]. The protonation–deprotonation of the N-H unit guides the mode of coordination of the hydrazone ligand to the metal centre, which may lead to N∩O or N∩N coordination. Apart from this bonding property, hydrazone derivatives have been reported to exhibit a number of biological properties such as anti-bacterial [9], anti-cancer, DNA binding and cleavage activity studies [10-13]. The properties possessed by the platinum group metals and the hydrazone derivative ligands curved our minds to synthesize and investigate the properties of these complexes, which could prove beneficial in the field of pharmaceuticals.

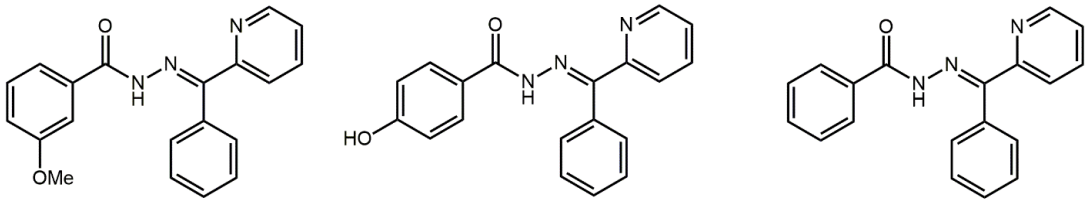

Chart 1: Ligands used in this study.

Experimental

Materials and Methods

The reagents α-phellandrene, pentamethylcyclopentadiene were purchased from Sigma Aldrich. 2-Benzoyl pyridine, 3-methoxy benzhydrazide, 4-hydroxy benzhydrazide and benzhydrazide were purchased from Spectrochem and Alfa Aesar. The reagents were of good commercial quality and were used without further purification. The solvents used for synthesis were dried and distilled prior to use according to the standard procedures [14]. The precursor ruthenium complex $[(arene)RuCl_2]_2$ was synthesized following the reported procedure [15] and $[Cp^*MCl_2]_2$ (M = Rh/Ir) complexes were prepared using a synthesizer, Anton par mono-wave 50 [16].

The synthesized complexes were characterized by various spectroscopic techniques such as FT-IR, ^1H NMR, ^{13}C NMR, ESI-Mass spectroscopy, UV-Vis, and Single-Crystal X-ray diffraction techniques. NMR spectra were recorded on a Bruker Advance II 400 MHz spectrometer using $CDCl_3$ for ^1H NMR and $CDCl_3$/DMSO (except complex **3** only $CDCl_3$ was used) for ^{13}C NMR as solvents. TMS was used as a standard reference. Infrared spectra (KBr pellets; 400-4000 cm^{-1}) were recorded on a Perkin-Elmer 983 spectrophotometer. Mass spectra were recorded with Q-T of APCI-MS instrument (model HAB 273) and micrOTOF-Q II 10337 using acetonitrile as the

solvent. The absorption spectra for the complexes were recorded on a Perkin-Elmer Lambda 25 UV-Vis spectrophotometer in the range of 200-600 nm using acetonitrile at room temperature.

Structure determination by X-ray Crystallography

Oxford Diffraction Xcalibur Eos Gemini diffractometer using graphite monochromatic Mo-Kα radiation (λ = 0.71073 Å) was used to collect the molecular structures of the complexes. The approach for the data collection was calculated using the CrysAlisPro CCD software. Crystal data was collected using Standard ‘‘phi–omega scan’’ techniques and the data was scaled and reduced using CrysAlisPro RED software. The structure solution of the complexes was carried out by SHELXT and refined by full-matrix least squares method based on F^2 against all reflections using SHELXL-2014 and SHELXL-2016 [17]. Metal atoms in the complexes were located from E-maps and all non-hydrogen atoms were refined anisotropically by full-matrix least-squares. Hydrogen atoms were placed in geometrically idealized positions and constrained to ride on their parent atoms with C-H distances in the range 0.95-1.00 Å. Isotropic thermal parameters U_{eq} were fixed such that they were 1.2 U_{eq} of their parent atom for CH's and 1.5 U_{eq} of their parent atom in case of methyl groups. Table 1, summarized the crystallographic and structure refinement parameters for the complexes and selected bond lengths and bond angles are presented in Table 2. The molecular structures were drawn using ORTEP-3 [18] and packing pattern and interactions like π-π, H- bonding can be obtained using MERCURY [19].

Antibacterial activity

All strains were tested for purity by standard microbiological methods. An agar-well diffusion method [20] was employed for the evaluation of anti-bacterial activities of the tested compounds.The agar nutrient broth media was prepared, sterilized at 121°C for 15 min. The

chosen bacterial strains were inoculated in nutrient broth and incubated overnight. Petri-plates containing 30 mL of fresh Muller Hinton (MH) agar medium was seeded with 24 hour grown culture of bacterial strains. Wells of 5 mm diameter were cut and 100 μL of each compound was added. The plates were then incubated at 37 °C for 72 hours. The antibacterial activity was evaluated by measuring the diameter of the inhibition zone formed around the well. Each well diffusion experiment was performed in triplicate with 1 mg mL^{-1} concentration of the compounds. Dimethylsulphoxide (DMSO) was used as a solvent and as a negative control, whereas kanamycin antibiotic was used as a positive control.

Cell lines testing, culture condition and cytotoxicity studies

The response of HCT116 p53 wild type ($p53^{+/+}$) and HCT116 p53 null ($p53^{-/-}$) human colorectal cancer lines [21] to the tested compounds was determined following continuous 96-hour exposure using the MTT assay. To compare the activity of the compounds against cancer cells to non-cancer cells, compounds were also evaluated against the retinal epithelium cell line ARPE-19. HCT116 cells were kindly provided by Professor Bert Vogelsteins (John Hopkins University, Baltimore, MD) and ARPE-19 cells were originally purchased from ATCC. HCT116 cells were routinely maintained as monolayer cultures in DMEM media supplemented with 10% foetal calf serum and L-glutamine (2 mM). ARPE-19 cells were routinely maintained as monolayer cultures in DMEM:F12 medium supplemented with 10% foetal calf serum, L-glutamine (2.5 mM) and sodium pyruvate (0.5 mM).

The antiproliferative activity of the compounds was evaluated using the MTT (3-(4,5-dimethylthiazol-2-yl)-2,5-diphenyltetrazolium bromide) cellular viability assay as described elsewhere [22]. Briefly cells were seeded into 96 well plates at 2 x 10^3 cells per well and incubated for 24 hours at 37°C in an atmosphere of 5% CO_2 prior to drug exposure. Generally, a

stock solution of each compound was freshly prepared in DMSO at a concentration of 100 mM. The highest concentration of drug tested was 100 μM and the final DMSO concentration applied to cells was 0.1% (v/v), which is nontoxic to cells. The cells were exposed to a range of drug concentrations for 96 hours and cell survival was determined using the MTT assay. Following drug exposure, 20 μL of MTT (0.5 mg/mL) in phosphate buffered saline was added to each well and it was further incubated at 37 °C for 4 hours in an atmosphere containing 5% CO_2. The solution was removed and formazan crystals were dissolved in 150 μM DMSO. The absorbance of the resulting solution was recorded at 550 nm using an ELISA spectrophotometer. The percentage cell survival was calculated by dividing the true absorbance of treated cultures by the true absorbance for controls (exposed to 0.1% DMSO). Results are presented as the mean IC_{50} (μM) ± standard deviation for three independent experiments. To compare the response of non-cancer cells to cancer cells, the selectivity index (SI) was also calculated which is defined as the IC_{50} for ARPE19 cells divided by the IC_{50} for each cancer cell line. Values >1 indicate that compounds have selective activity against cancer compared to non-cancer cells *in vitro*. Previously published data for cisplatin [23] is also reported here to provide comparative results.

General procedure for synthesis of metal complexes (1-9)

All the metal complexes were prepared by reacting metal precursors $[(arene)MCl_2]_2$ (0.1 mmol) and benzhydrazone derivative ligands (**L1, L2** and **L3**) (0.2 mmol) in dry methanol (10 mL) and stirred at room temperature for 1hour (Schemes 1 and 2) after which NH_4PF_6 was added and the solution was further stirred for additional 3 hours. After the completion of the reaction, the solvent was fully evaporated under reduced pressure and residue was dissolved in dichloromethane and filtered to remove NH_4Cl through celite. The solution was then concentrated to 1-2 mL and the compound was precipitated out using hexane/diethyl ether

yielding orange-yellow compounds. The precipitate was then washed with diethyl ether and air-dried. All these complexes were of good yield, pure and were found to be soluble in polar solvents but insoluble in non-polar solvents.

[(*p*-cymene)Ru(L1)Cl]PF_6 (1)

Yield: (75%); dark yellow; FT-IR (KBr, cm^{-1}): 3346$\nu_{(NH)}$, 1628$\nu_{(C=O)}$, 842$\nu_{(P-F)}$; ^{1}H NMR (400 MHz, $CDCl_3$, ppm) = 8.81 (d, 1H, *J* = 4 Hz), 8.14 (s, 1H), 7.98 (s, 1H), 7.92 (t, 1H, *J* = 8 Hz), 7.72 (broad singlet, 4H) 7.63-7.56 (m, 2H), 7.54 (s,1H), 7.48 (t, 1H, *J* = 8Hz), 7.22 (d, 1H, *J* = 8 Hz), 7.08 (d, 1H, *J* = 8 Hz), 5.66 (d, 1H, *J* = 8 Hz)$_{(p\text{-cym})}$, 5.44 (d, 1H, *J* = 4 Hz)$_{(p\text{-cym})}$, 5.19 (d, 1H, *J* = 8 Hz)$_{(p\text{-cym})}$, 3.65 (d, 1H, *J* = 4 Hz)$_{(p\text{-cym})}$, 3.92 (s, 3H), 2.89-2.81 (sept, 1H)$_{(p\text{-cym})}$, 2.11 (s, 3H)$_{(p\text{-cym})}$, 1.23 (s, 3H)$_{(p\text{-cym})}$, 1.18 (d, 3H, *J* = 8 Hz)$_{(p\text{-cym})}$; MS-ESI (m/z): calculated: 566.14 [M-PF_6-HCl]$^+$, found: 566.08; UV-Vis {Acetonitrile, λ_{max} nm ($\varepsilon/10^{-4}$ M^{-1} cm^{-1})}: 270 (1.522), 322 (1.563).

[Cp*Rh(L1)Cl]PF_6 (2)

Yield: (72%); orange; FT-IR (KBr, cm^{-1}): 3409$\nu_{(O-H)}$, 1634$\nu_{(C=N-N=C)}$, 844$\nu_{(P-F)}$; ^{1}H NMR (400 MHz, $CDCl_3$, ppm) = 10.21 (s, 1H), 8.92 (d, 1H, *J* = 4 Hz), 8.84 (d, 1H, *J* = 4 Hz), 8.04 (t, 1H, *J* = 8 Hz), 7.90 (t, 1H, *J* = 8 Hz), 7.84 (t, 1H, *J* = 8 Hz), 7.64 (d, 2H, *J* = 4 Hz), 7.56-7.48 (m, 4H), 7.35 (d, 1H, *J* = 4 Hz), 7.06 (d, 1H, *J* = 8 Hz), 3.80 (s, 3H), 1.75 (s, 15H, Cp*); ^{13}C NMR (100 MHz, $CDCl_3$ + DMSO-d_6, ppm) = 177.14, 162.00, 159.36, 152.94, 152.40, 139.81, 131.86, 131.07, 129.86, 129.67, 128.72, 128.43, 127.07, 119.43, 118.08, 112.67, 98.58, 98.50, 55.21, 8.80; MS-ESI (m/z): calculated: 568.15 [M-PF_6-HCl]$^+$, found: 568.29; UV-Vis {Acetonitrile, λ_{max} nm ($\varepsilon/10^{-4}$ M^{-1} cm^{-1})}: 225 (3.094), 271 (1.462), 326 (1.119).

[Cp*Ir(L1)Cl]PF_6 (3)

Yield: (65%); yellow; FT-IR (KBr, cm^{-1}): 3433$\nu_{(O-H)}$, 1638$\nu_{(C=N-N=C)}$, 844$\nu_{(P-F)}$; ^{1}H NMR (400 MHz, $CDCl_3$, ppm) = 9.91 (s, 1H), 8.92 (d, 1H, *J* = 8 Hz), 8.07 (t, 1H, *J* = 8 Hz), 8.03 (d, 1H, *J* = 8 Hz), 7.91 (t, 1H, *J* = 8 Hz), 7.71-7.60 (m, 3H), 7.56-7.52 (m, 1H), 7.44 (t, 2H, *J* = 8 Hz), 7.34-7.32 (m, 2H), 7.07 (t, 1H, *J* = 8 Hz), 3.80 (s, 3H), 1.73 (s, 15H, Cp*); ^{13}C NMR (100 MHz, $CDCl_3$, ppm) = 178.31, 161.56, 159.82, 159.56, 158.44, 153.80, 153.05, 152.03, 140.15, 131.55, 130.33, 129.77, 128.92, 128.67, 120.16, 119.21, 119.07, 118.48, 112.70, 112.16, 91.71, 55.46, 8.71; MS-ESI (m/z): calculated: 658.20 [M-PF_6-HCl]$^+$, found: 658.28; UV-Vis {Acetonitrile, λ_{max} nm ($\varepsilon/10^{-4}$ M^{-1} cm^{-1})}: 282 (1.589), 386 (0.377).

[(*p*-cymene)Ru(L2)Cl]PF_6 (4)

Yield: (80%); yellow; FT-IR (KBr, cm^{-1}): 3452$\nu_{(O-H)}$, 3280$\nu_{(N-H)}$, 1642$\nu_{(C=O)}$, 844$\nu_{(P-F)}$; ^{1}H NMR (400 MHz, $CDCl_3$, ppm) = 12.20 (s, 1H), 9.08 (s, 1H), 8.12 (t, 1H, *J* = 8 Hz), 7.94 (s, 3H), 7.89 (s, 2H), 7.89 (s, 2H), 7.79-7.72 (m, 2H), 7.16 (d, 1H, *J* = 8 Hz), 7.02 (d, 3H, *J* = 8 Hz), 6.92 (d, 1H, *J* = 8 Hz), 5.67 (d, 2H, *J* = 8 Hz)$_{(p\text{-cym})}$, 5.44 (d, 2H, *J* = 8 Hz)$_{(p\text{-cym})}$, 2.78-2.74 (sept, 1H)$_{(p\text{-cym})}$, 2.13 (s, 3H)$_{(p\text{-cym})}$, 1.22 (d, 6H, *J* = 8 Hz)$_{(p\text{-cym})}$; ^{13}C NMR (100 MHz, $CDCl_3$ + DMSO-d_6, ppm) = 171.73, 163.64, 157.63, 150.12, 146.25, 136.85, 130.55, 130.28, 129.53, 127.09, 116.13, 103.10, 80.67, 78.94, 30.33, 21.70, 21.53, 18.22; MS-ESI (m/z): calculated: 552.14 [M-PF_6-HCl]$^+$, found: 552.12; UV-Vis {Acetonitrile, λ_{max} nm ($\varepsilon/10^{-4}$ M^{-1} cm^{-1})}: 245 (0.952), 329 (0.933).

[Cp*Rh(L2)Cl]PF_6 (5)

Yield: (88%); orange; FT-IR (KBr, cm^{-1}):3436$\nu_{(O-H)}$, 1643$\nu_{(C=N-N=C)}$, 846$\nu_{(P-F)}$; ^{1}H NMR (400 MHz, $CDCl_3$, ppm) = 12.64 (s, 1H), 9.01 (d, 1H, *J* = 4 Hz), 8.14 (t, 1H, *J* = 8 Hz), 8.01-7.95 (m, 1H), 7.70 (d, 1H, *J* = 8 Hz), 7.58-7.51 (m, 5H), 7.47-7.39 (m, 4H), 7.30 (d, 1H, *J* = 8 Hz), 1.75 (s, 15H, Cp*); ^{13}C NMR (100 MHz, $CDCl_3$ + DMSO-d_6, ppm) = 175.87, 162.25, 161.21, 153.07, 152.34, 139.81, 130.57, 129.56, 129.36, 128.56, 128.34, 128.06, 126.81, 121.17, 114.87, 98.03, 97.96, 8.62; MS-ESI (m/z): calculated: 554.13 $[M-PF_6-HCl]^+$, found: 554.13; UV-Vis {Acetonitrile, λ_{max} nm ($\varepsilon/10^{-4}$ $M^{-1}cm^{-1}$)}: 233 (2.368), 275 (1.426), 327 (1.040).

[Cp*Ir(L2)Cl]PF_6 (6)

Yield: (79%); yellow; FT-IR (KBr, cm^{-1}): 3504$\nu_{(O-H)}$, 1607$\nu_{(C=N-N=C)}$, 846$\nu_{(P-F)}$; ^{1}H NMR (400 MHz, $CDCl_3$, ppm) = 11.99 (s, 1H), 8.96 (d, 1H, *J* = 4 Hz), 8.09-8.01 (m, 3H), 7.86 (t, 1H, *J* = 8 Hz), 7.61 (d, 3H, *J* = 8 Hz), 7.54 (d, 2H, *J* = 4 Hz), 7.34 (d, 1H, *J* = 4 Hz), 7.03-7.00 (m, 1H), 6.84-6.82 (m, 2H), 1.71 (s, 15H, Cp*); MS-ESI (m/z): calculated: 644.19 $[M-PF_6-HCl]^+$, found: 644.18; UV-Vis {Acetonitrile, λ_{max} nm ($\varepsilon/10^{-4}$ M^{-1} cm^{-1})}: 246 (1.785), 272 (1.660), 326 (1.770).

[(*p*-cymene)Ru(L3)Cl]PF_6 (7)

Yield: (82%); yellow; FT-IR (KBr, cm^{-1}): 3090$\nu_{(N-H)}$, 1599$\nu_{(C=O)}$, 839$\nu_{(P-F)}$; ^{1}H NMR (400 MHz, $CDCl_3$): (ppm) = 8.86 (d, 1H, *J* = 4 Hz), 8.11 (s, 1H), 8.08 (d, 3H, *J* = 8 Hz), 7.94 (t, 1H, *J* = 8 Hz), 7.73-7.68 (m, 5H), 7.65-7.57 (m, 3H), 7.09 (d, 1H, *J* = 8 Hz), 5.65 (d, 1H, *J* = 8 Hz)$_{(p\text{-cym})}$, 5.43 (d, 1H, *J* = 4 Hz)$_{(p\text{-cym})}$, 5.23 (d, 1H, *J* = 8 Hz)$_{(p\text{-cym})}$, 3.62 (d, 1H, *J* = 8 Hz), 2.90-2.80 (sept, 1H)$_{(p\text{-cym})}$, 2.11 (s, 3H)$_{(p\text{-cym})}$, 1.24 (d, 3H, *J* = 8 Hz)$_{(p\text{-cym})}$, 1.18 (d, 3H, *J* = 8 Hz)$_{(p\text{-cym})}$; ^{13}C NMR (100 MHz, $CDCl_3$ + DMSO-d_6, ppm) = 172.70, 158.27, 149.61, 145.63, 139.81, 136.64, 134.21, 130.63, 129.67, 128.98, 127.83, 127.26, 125.87, 103.61, 101.88, 86.27, 85.16, 84.58, 80.70, 79.31, 78.86, 30.32, 21.65, 21.59, 21.16, 18.18; MS-ESI (m/z): calculated: 536.13 [M-PF_6-

HCl]$^+$, found: 536.33; UV-Vis {Acetonitrile, λ_{max} nm ($\varepsilon/10^{-4}$ M^{-1} cm^{-1})}: 235 (1.571), 267 (1.266), 318 (1.283).

[Cp*Rh(L3)Cl]PF_6 (8)

Yield: (85%); orange; FT-IR (KBr, cm^{-1}): 3447$\nu_{(O-H)}$, 1620$\nu_{(C=N-N=C)}$, 844$\nu_{(P-F)}$; ^{1}H NMR (400 MHz, $CDCl_3$, ppm) = 10.23 (s, 1H), 8.95 (d, 1H, *J* = 8 Hz), 8.09-8.01 (m, 2H), 7.92 (d, 1H, *J* = 8 Hz), 7.86 (d, 2H, *J* = 8 Hz), 7.64 (t, 2H, *J* = 4 Hz), 7.51 (t, 3H, *J* = 8 Hz), 7.42 (d, 3H, *J* = 8 Hz), 1.73 (s, 15H, Cp*); MS-ESI (m/z): calculated: 538.14 [M-PF_6-HCl]$^+$, found: 538.15; UV-Vis {Acetonitrile, λ_{max} nm ($\varepsilon/10^{-4}$ M^{-1} cm^{-1})}: 230 (2.959), 328 (0.637), 390 (0.417).

[Cp*Ir(L3)Cl]PF_6 (9)

Yield: (70%); light yellow; FT-IR (KBr, cm^{-1}): 3447$\nu_{(O-H)}$, 1627$\nu_{(C=N-N=C)}$, 843$\nu_{(P-F)}$; ^{1}H NMR (400 MHz, $CDCl_3$, ppm) =9.93 (s, 1H), 8.96 (d, 1H, *J* = 4 Hz), 8.06-8.01 (m, 1H), 7.83 (d, 2H, *J* = 4 Hz), 7.74-7.70 (m, 2H), 7.60-7.52 (m, 5H), 7.47 (broad singlet, 3H), 1.63 (s, 15H, Cp*); MS-ESI (m/z): calculated: 628.19 [M-PF_6-HCl]$^+$, found: 628.19; UV-Vis {Acetonitrile, λ_{max} nm ($\varepsilon/10^{-4}$ M^{-1} cm^{-1})}: 268 (1.484), 317 (1.554).

Results and discussion

Synthesis of metal complexes

The metal complexes **1-9** have been synthesized by reacting metal precursors and the respective hydrazone ligands **L1**, **L2** and **L3** in dry methanol for 4 hours in the ratio of 1:2 (Schemes1 and 2). All these complexes have been isolated as cationic bidentate complexes with PF_6 as the counter ion. Previous reports illustrated that [24], ruthenium complexes of hydrazone derivatives exhibited N∩O coordination mode as neutral complexes by deprotonation of the N-H proton

using base such as Et_3N. In several studies, ruthenium with benzhydrazone ligands, readily forms N∩N bonding mode but in this case, ruthenium complexes exhibited N∩O bonding mode even without the usage of a base while for rhodium and iridium complexes, N∩O bonding mode is expected but the reverse is observed. All these complexes were isolated in good yield, air stable and soluble in polar solvents like dichloromethane, chloroform, methanol, acetonitrile, DMSO but insoluble in hexane, pet ether and diethyl ether.

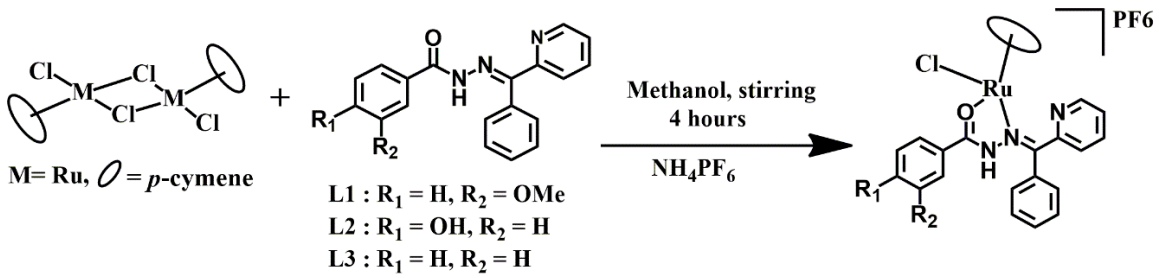

Scheme 1: Synthesis of ruthenium complexes.

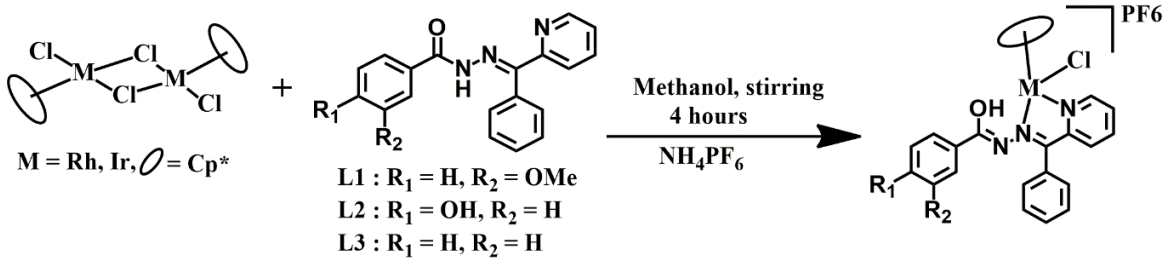

Scheme 2: Synthesis of rhodium and iridium complexes.

Description of molecular structures of metal complexes

Crystallographic study proves to be a strong ratification for the formation of the metal complexes which also gives in depth information of the coordination and various bonding bonds in metal complexes, where other spectroscopic methods are unable to do so. The ORTEP representation of the isolated crystal structures **1**, **2**, **3**, **4**, **5** and **7** with atom numbering are presented in Figures 1-3. Complex **2** because of low theta value, have been given just to show the coordination of the

ligand to the metal centre and the relevant crystallographic parameters are listed in Table 1. Single crystals of the complexes were attached to a glass fibre and transferred to the Oxford Diffraction Xcalibur Eos Gemini diffractometer. X-ray analysis revealed and confirmed the complexes are cationic bearing the general formula [(arene)M(L)Cl]PF_6. The metal complexes highlighted a regular three-legged "piano stool" geometry in which the arene ring (arene =*p*-cymene, Cp*) occupied the facial coordination sites at the metal in η^5/η^6 manners, terminal chloride and chelating N∩O donor ligand in case of ruthenium complexes and N∩N donor ligand in case of rhodium and iridium complexes. The d^6 metal atom shows pseudo octahedral geometry with the arene ring occupying the three facial geometry acting as the seat of a piano and the donor atoms from benzhydrazone derivatives and chloride atom acting as the three legs of a piano. The molecular structures of these complexes revealed the benzhydrazone derivative ligands preferably bind to the ruthenium metal in a bidentate manner through nitrogen and oxygen donor atoms but to the rhodium and iridium metals, the ligands bind through the nitrogen of the pyridine ring and the imine nitrogen which at the same time, migration of the adjacent N-H hydrogen was observed which led to keto-enol tautomerism of the C=O group. Complexes **1** and **7**, crystallized in triclinic system with space group '$P\bar{1}$'while complex **4** crystallized in monoclinic system with space group '*Pc'* respectively while complex **2**, **3** and **5** crystallized in orthorhombic systems with space group '*Pccn'* (for complexes **2** and **3**) and '$Pca2_1$' (for complex **5**). The representative bond distances as well as the bond angle values are given in Table 2. The M-Cl bond lengths in these complexes are found to be comparable to the previous reported values.

The N∩N chelating complexes showed intra Cl-----O interactions (Figures 4-5) which gives more stability to the complexes formed when the NH proton migrates to the carbonyl group. The

measured distances of Cl(1)------O(1) of the representative complexes **2**, **3** and **5** are 3.031 Å, 3.039 Å and 2.966 Å respectively.

FT-IR study

IR spectra revealed the presence of functional groups present in the ligands as well as in the complexes. The stretching frequency of N-H group in ruthenium complexes can be clearly observed in the range 3090-3346 cm^{-1}, this peak was absent in the rhodium and iridium complexes but additional peak due to OH group at 3409-3504 cm^{-1} was observed which suggested keto-enol tautomerism. The stretching frequency of C=O in case of the ligands was found to be in the range of 1620-1642 cm^{-1} while in the case of ruthenium complexes, the stretching frequency of C=O was found to be in the range of 1599-1642 cm^{-1}. This small decrease in the stretching frequency of C=O group can be attributed to the fact that there is a coordination to the metal centre through the oxygen of carbonyl group, while in the case of the rhodium and iridium complexes, a band in the range of 1607-1643 cm^{-1} was observed which corresponded to the azomethine group (-C=N-N=C-) formed from the migration of the N-H proton to the oxygen atom of C=O group forming enol [6]. Since the complexes were isolated as PF_6 salts, the presence of PF_6 can be confirmed by the appearance of P-F band at 839-846 cm^{-1}.

^{1}H NMR spectroscopy

The ^{1}H NMR spectra of the complexes have been provided in the supplementary information **(**Figures S1-S7). NMR spectroscopy confirms the coordination of the ligands with the metal precursors showing the appearance of the ligand proton signals as well as *p*-cymene and Cp* ring protons. The number of proton signals expected was found to tally with that found from the NMR spectra. The N-H signals were observed in the aromatic region along with aromatic

protons of the ligands. It was observed that in case of the rhodium and iridium complexes, the proton of O-H group formed by the migration of the adjacent N-H proton to the C=O forming enol group was found to be in the range 8.96-10.23 ppm, but in the case of complexes **4**, **5** and **6** due to the co-existing O-H group in the free ligand (**L2**), a downfield peak was observed in the range 11.99-12.64 ppm. In ruthenium complexes, an unusual splitting pattern of signal for *p*-cymene moiety was noted where, in complexes **1** and **7**, the aromatic proton signals of *p*-cymene splits into four doublets in the range 3.62-5.66 ppm, while in complex **4**, two doublets around 5.67 ppm and 5.44 ppm. Regarding the six-methyl protons of *p*-cymene, complexes **1** and **7** showed similar splitting pattern where two doublets in the range 1.18-1.24 ppm was observed instead of one doublet, while complex **4** showed a single signal at 1.22 ppm. This unusual pattern is due to the diastereotopic nature of the metal centre [25]. A septet of the isopropyl proton for complexes **1, 4, 7** was observed around 2.81-2.89 ppm, 2.74-2.78 ppm and 2.80-2.90 ppm respectively and a singlet of the methyl proton at the *para*-position of the *p*-cymene ring was observed at 2.11 ppm, 2.13 ppm and 2.11 ppm respectively. Similarly, in rhodium and iridium complexes, in addition to the proton peaks of the ligands, we also observed a sharp singlet around 1.63-1.75 ppm for complexes **2**, **3**, **5**, **6**, **8** and **9** corresponding to Cp* protons. Therefore, the presence of the expected peaks and integration from the NMR study confirmed the formation of the complexes.

^{13}C NMR spectroscopy

The formation of complexes is further substantiated by ^{13}C NMR data. The spectra of the representative complexes were given in the supplementary data (Figures S8-S12). The aromatic carbon peaks of the ligands were observed around 112.16-178.31 ppm. A singlet peak of the carbonyl carbon appeared in the range 171.79-172.70 ppm while the carbon of the C-OH group

appeared around 175.87-178.31 ppm which was formed by the migration of the N-H proton. The peak corresponding to the carbon attached to OH group at the *para*-position (complexes of **L2**) and to OMe at the *meta* position (complexes of **L1**) was observed in the range 162.25-163.64 ppm and carbon peak of C=N was observed in the range 157.63- 161.21 ppm. The peak around 55.20-55.46 ppm was assigned to the carbon of the methoxy group -OCH_3. The *p*-cymene ring carbons were observed around 78.94-103.31 ppm while that of the methyl, methine and isopropyl carbons were observed around 18.18-30.32 ppm respectively. The methyl carbons of the Cp* ring were observed around 7.59-8.80 ppm and the ring carbons were observed at 91.71-98.58 ppm. Overall, these results support the formation of the complexes.

Mass studies of the complexes

Mass data of all the complexes **1-9** are provided in the supplementary data (Figures S13-S21) and their values are given in the experimental section. The masses of the complexes analysed were found to be consistent and accorded with the calculated masses. Some of the complexes, in addition to the molecular ion peaks, showed other isotopic peaks too by addition/ loss of protons. The molecular ion peaks of the analysed complexes were found to be in agreement with the calculated masses and for each complex, molecular ion peak is displayed at m/z: 566.08 (**1**), m/z: 568.29 (**2**), m/z: 658.28 (**3**), m/z: 552.12 (**4**), m/z: 554.13 (**5**), m/z: 644.18 (**6**), m/z: 536.33 (**7**), m/z: 538.14 (**8**), m/z: 628.19 (**9**) corresponding to $[M\text{-}PF_6\text{-}HCl]^+$. Complexes **2**, **3**, **4**, **5**, **6** and **9** showed corresponding isotopic masses as well. These ion peaks indicated by mass analysis of the complexes in comparison to the calculated mass, shows that there is a strong bonding of the arene ring (arene = *p*-cymene, Cp*) to the metal atom.

UV-Visible description of metal complexes

To learn about the electronic transitions of metal complexes, the electronic spectra of the metal complexes were recorded in acetonitrile with 10^{-4} M concentrations at room temperature and spectra are provided in the supplementary data (Figure S22). Since in these complexes, the metal atoms are d^6 low spin metal complexes and these metal atoms are at their most reduced oxidation state, they contain filled orbitals of proper geometry at the metal centres which can interact with the low-lying π* orbitals of the ligands which may result in metal-to-ligand charge transfer (MLCT) transitions. The metal-to-ligand charge transfer (MLCT) dπ(M) to π*(L) transitions which are the low energy absorption bands were observed in the range 317-390 nm while the high energy absorption bands were observed in the range 225-282 nm may be attributed to ligand-centred π- π*/ n- π* transfer [26].

In-vitro antibacterial assay

The synthesized complexes **1**-**9** along with the ligands were evaluated for *in-vitro* antibacterial activity against Gram-positive Bacteria *i.e., S. aureus* and *B. thuringiensis* and Gram-negative Bacteria *E. coli* and *P. aeruginosa* by using standard techniques [27]. The zones of inhibition (mm) in comparison to kanamycin are given in Figure S23, Table S1 and Figure 6. Out of all the compounds tested, only ligand **L2** and complex **5** exhibited potent antibacterial activity against the tested organisms. *In-vitro* assay results revealed that ligand **L2** (16 ± 2 mm) showed good activity against Gram-positive (*B. thuringiensis*) as well as potent activity towards Gram-negative bacteria with an inhibition value of 15 ± 2 mm and 14 ± 2 mm towards *E. coli* and *P. aeruginosa* respectively. Complex **5** showed activity only towards the Gram-negative Bacteria *E. coli* and *P. aeruginosa* with zone of inhibition 16 ± 1 respectively. On comparing the activity of complex **5** and ligand **L2**, they have more or less comparable activities towards the bacterial strains which could suggest that the antibacterial activity comes mainly from the ligand moiety

(where O-H group is present) and unique property of rhodium metal centre as to ruthenium and iridium metal centres. Whilst the activity of complexes is less than the antibacterial activity of the standard kanamycin, the activity of ligand **L2** and its rhodium complex is nevertheless a promising potential lead for the future development of this class of compound as antibacterial drugs.

Cytotoxicity studies

The response of cell lines to cisplatin and test compounds is presented in Figure 7 and Table 3. For both HCT116p53$^{+/+}$ and HCT116 p53$^{-/-}$ cell lines, a broad range of IC_{50} values were obtained with IC_{50} values ranging from 0.695 ± 0.017 (ligand **L3**) to 6.23 ± 0.08 μM (complex **3**). In contrast to cisplatin, both p53 wild type and p53 null cells were equally sensitive to test compounds. The response of non-cancer ARPE-19 cells ranged from 1.67 ± 0.75 (complex **7**) to >100 μM (complexes **4-6**). From the cytotoxic studies of the complexes of the respective ligands, rhodium complexes were found to show more anticancer activity towards the cancer cells studied which could be attributed to various properties of the rhodium precursors such as the size of the metal and the symmetrical geometry of the arene ring. Selectivity indices (SI) are presented in Figure 8 and Table 4 and for complexes **3**, **7** and **8**, SI values slightly above or below 1 were obtained. Whilst SI values increased for ligand **L1**, complexes **1**, **2** and ligand **L3** (up to an SI value of 2.84 for complex **2**), the highest SI values were obtained for ligand **L2** and complexes **4-6**. Note that the SI values for ligand **L2** and complexes **4-6** are estimates as the IC_{50} values were >100 μM which was the highest dose tested. Ligand **L2** and complex **5** are of particular interest in that they have superior potency than cisplatin *in vitro* but have significantly enhanced selectivity for HCT116 cancer cells as opposed to non-cancer ARPE-19 cells.

The high potency of the ligand **L2** and complexes **4-6** as compared to other ligands (**L1** and **L3**) and their complexes could be attributed to the presence of the O-H group at the para-position of the benzhydrazide moiety which may enhances the solubility of the compound and reactivity.

Conclusion

In summary, the synthesized complexes have been successfully characterized by various spectroscopic techniques and studied for their biological activity. All these complexes were found to be cationic in nature with PF_6 as the counter ion, where the ligands bind to the metal centrein a bidentate chelating manner. In the case of ruthenium complexes, the hydrazone derivative ligands bind preferably through the imine nitrogen and the carbonyl oxygen but in the case of rhodium and iridium complexes, the ligands bind to the metal centres through the imine nitrogen and the pyridyl nitrogen with the migration of the adjacent N-H proton which is a common case of the hydrazone derivatives forming keto-enol tautomerism. Due to low symmetry crystal data, the ORTEP diagram of complex 8 presented as Figure S24 to know the bonding modes. The biological studies demonstrated that ligand **L2** and complex **5** showed significant anti-bacterial activity against Gram-positive (*B. thuringiensis*) and Gram-negative bacteria (*E. coli* and *P. aeruginosa***)**. Also, ligand **L2** and complex **5** were more potent than cisplatin against HCT116 colorectal carcinoma cells *in vitro* but importantly, greater selectivity towards cancer as opposed to non-cancer cells than cisplatin was demonstrated under identical experimental conditions.

Acknowledgements

Lathewdeipor Shadap thanks CSIR, New Delhi, India for providing financial assistance in the form of JRF, DST-PURSE SCXRD, NEHU-SAIF, Shillong, India for providing Single Crystal X-ray analysis and other spectral studies.

Appendix A. Supplementary data

CCDC 1943881 (**1**), 1943880 (**3**), 1943884 (**4**), 1943882 (**5**) and 1943883 (**7**) contains the supplementary crystallographic data for this paper. These data can be obtained free of charge via www.ccdc.cam.ac.uk/data_request/cif, by e-mailing data_request@ccdc.cam.ac.uk, or by contacting The Cambridge Crystallographic Data Centre, 12, Union Road, Cambridge CB2 1EZ, UK; Fax: +44 1223 336033.

References

[1] N. Mohan, M.K.M. Subarkhan, R. Ramesh, J. Organomet. Chem. 859 (2018) 124-131.

[2] T. Hirayama, S. Ueda, T. Okada, N. Tsurue, K. Okuda, H. Nagasawa, Chem. Eur. J. 20 (2014) 4156-4162.

[3] J. Klingele, D. Kaase, J. Hilgert, G. Steinfeld, M.H. Klingele, J. Lach, Dalton Trans 39 (2010) 4495-4507.

[4] R.N. Patel, Y. Singh, Y.P. Singh, A.K. Patel, N. Patel, R. Singh, R.J. Butcher, J.P. Jasinski, E. Colacio, M.A. Palaciose, New J. Chem. 42 (2018) 3112-3136.

[5] M. Kuriakose, M.R.P. Kurup, E. Suresh, Polyhedron 26 (2007) 2713-2718.

[6] I.P. Ferreira, E.D.L. Piló, A.A. Recio-Despaigne, J.G. Da Silva, J.P. Ramos, L.B. Marques, P.H.D.M. Prazeres, J.A. Takahashi, E.M. Souza-Fagundes, W. Rocha, H. Beraldo, Bioorg. Med. Chem. 24 (2016) 2988-2998.

[7] M.M. Fousiamol, M. Sithambaresan, V.A. Smolenski, J.P. Jasinski, M.R.P. Kurup, Polyhedron 141 (2018) 60-68.

[8] Y. Li, Z. Yang, M. Zhou, Y. Li, J. He, X. Wang, Z. Lin, RSC Adv. 7 (2017) 41527-41539.

[9] R. Pettinari, C. Pettinari, F. Marchetti, C.M. Clavel, R. Scopelliti, P.J. Dyson, Organometallics 32 (2012) 309-316.

[10] K.J. Kilpin, P.J. Dyson, Chem. Sci. 4 (2013) 1410-1419.

[11] P.K. Singh, D.N. Kumar, Spectrochim. Acta Part A 64 (2006) 853-858.

[12] B. Singh, R. Srivastava, K.K. Narang, Synth. React. Inorg. Met. Org. Chem. 30 (2000) 1175-1192.

[13] V. Onnis, M.T. Cocco, R. Fadda, C. Congiu, Bioorg. Med. Chem. 17 (2009) 6158-6165.

[14] W.L. Armarego, C.L. Chai (2013), Purification of laboratory chemicals, Butterworth-Heinemann.

[15] M.A. Bennett, T.N. Huang, T.W. Matheson, A.K. Smith, S. Ittel, W. Nickerson, Inorg. Synth. 21 (1982) 74-78.

[16] L. Shadap, S. Diamai, V. Banothu, D.P.S. Negi, U. Adepally, W. Kaminsky, M.R. Kollipara, J. Organomet. Chem. 884 (2019) 44-54.

[17] (a) G.M. Sheldrick, Acta Crystallogr. A 64 (2008) 112-122. (b) G.M. Sheldrick, Acta Crystallogr. C 71 (2015) 3-8.

[18] L.J. Farrugia, J. Appl. Crystallogr. 30 (1997) 565.

[19] C.F. Macrae, I.J. Bruno, J.A. Chisholm, P.R. Edgington, P. McCabe, E. Pidcock, L. Rodriguez-Monge, R. Taylor, J. van de Streek, P.A. Wood, J. Appl. Cryst. 41 (2008) 466–470.

[20] V. Banothu, A. Adepally, J. Lingam, Int. J Pharm. Pharm. Sci., 9 (2017) 192-198.

[21] F. Bunz, A. Dutriaux, C. Lengauer, T. Waldman, S. Zhou, J.P. Brown, J.M. Sedivy, K.W. Kinzler, B. Vogelstein, Science 282 (1998) 1497-1501.

[22] R.M. Phillips, P.B. Hulbert, M.C. Bibby, N.R. Sleigh, J.A. Double, Br. J. Cancer. 65 (1992) 359-364.

[23] R.A. Kaner, S.J. Allison, A.D. Faulkner, R.M. Phillips, D.I. Roper, S.L. Shepherd, D.H. Simpson, N.R. Waterfieldd, P. Scott, Chem. Sci. 7 (2016) 951-958.

[24] (a) K. Nagaraju, S. Pal, J. Organomet. Chem. 737 (2013) 7-11. (b) N. Raja, N. Devika, G. Gupta, V.L. Nayak, A. Kamal, N. Nagesh, B. Therrien, J. Organomet. Chem. 794 (2015) 104-114. (c) R.R Kumar, R. Ramesh, J.G.Małecki, J. Organomet. Chem. 862 (2018) 95-104.

[25] K.T. Prasad, B. Therrien, M.R. Kollipara, J. Organomet. Chem. 693 (2008) 3049-3056.

[26] S. Adhikari, W. Kaminsky, M.R. Kollipara, J. Organomet. Chem. 848 (2017) 95-103.

[27] NCCLS Performance standards for antimicrobial susceptibility testing. Ninth informational supplement. NCCLS document M100-S9. Wayne (PA): National Committee for Clinical Laboratory Standard (2008).

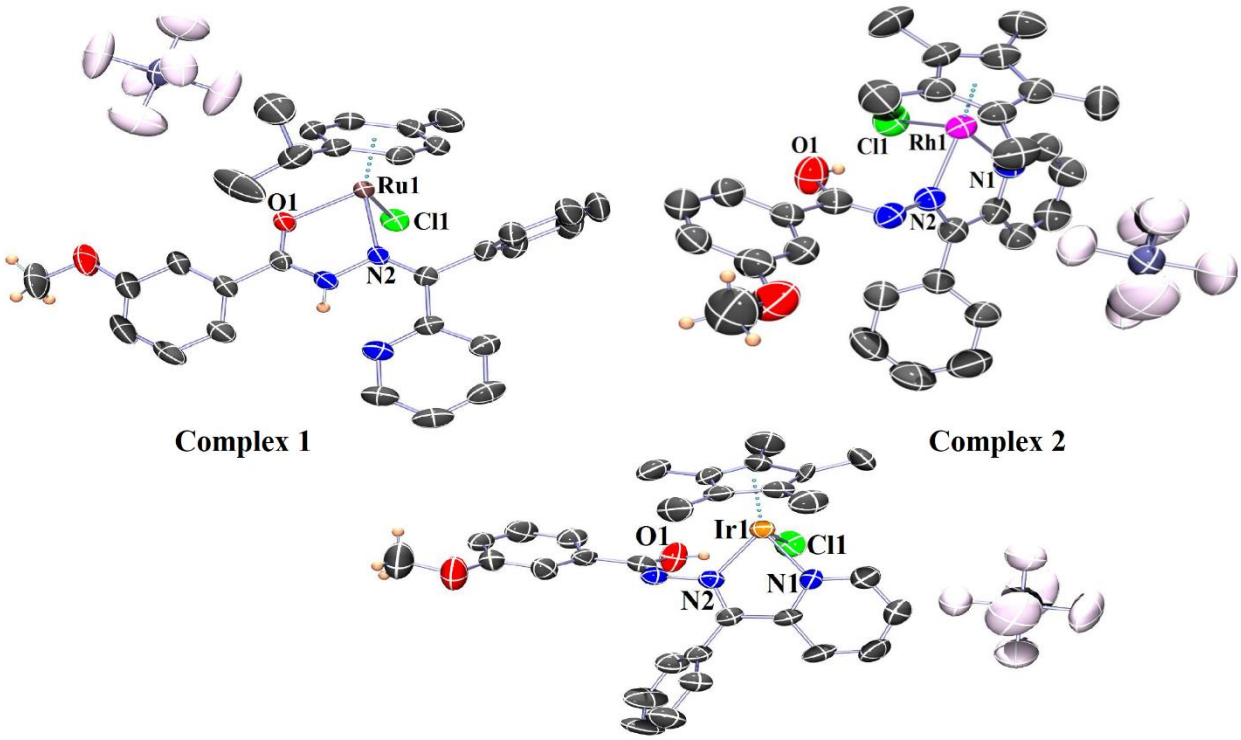

Figure 1: ORTEP diagrams of complexes **1**, **2** and **3** with 50% probability thermal ellipsoids. Complex **2** is just given here to show the composition and mode of bonding of the complex. Hydrogen atoms (except NH, OCH_3 and OH protons) have been omitted for clarity.

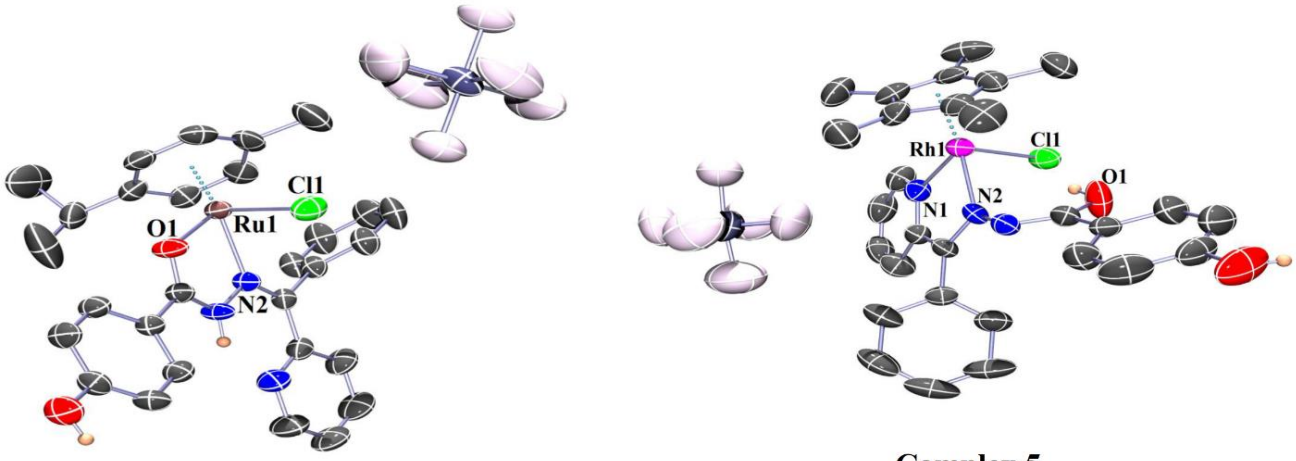

Complex 4 **Complex 5**

Figure 2: ORTEP diagrams of complexes **4** and **5** with 50% probability thermal ellipsoids. Hydrogen atoms (except NH and OH protons) have been omitted for clarity.

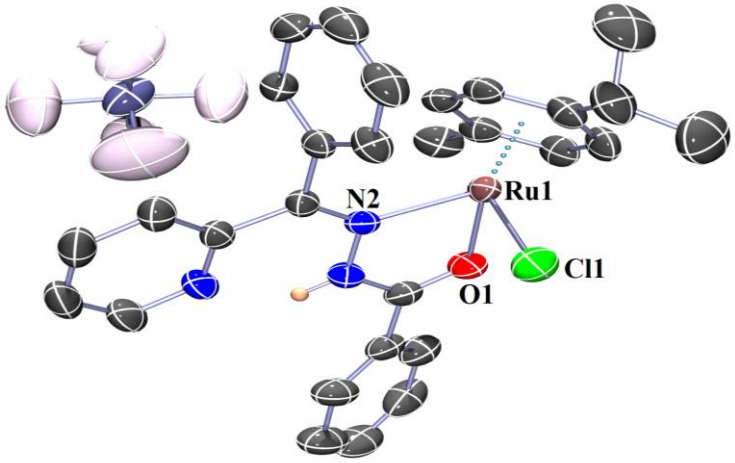

Figure 3: ORTEP diagram of complex **7** with 50% probability thermal ellipsoids. Hydrogen atoms (except NH proton) have been omitted for clarity.

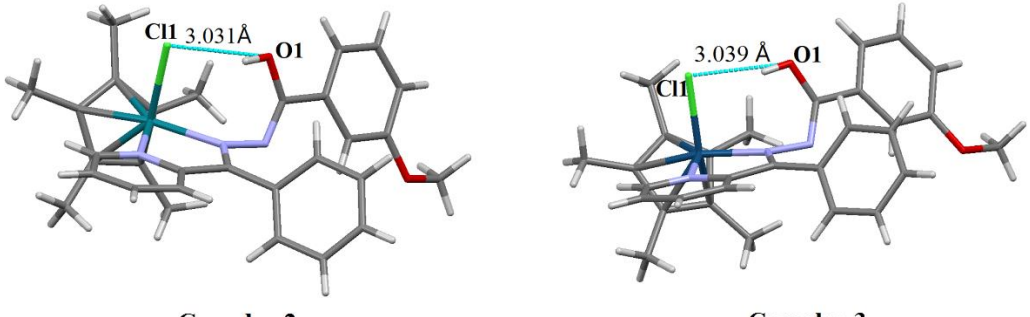

Complex 2 **Complex 3**

Figure 4: Intra Cl(1)----O(1) interaction of complexes **2** and **3**.

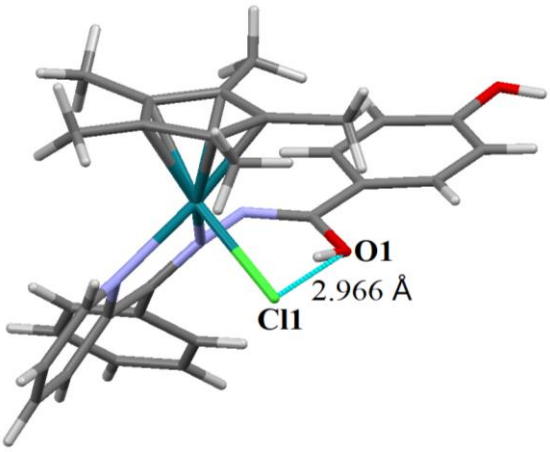

Figure 5: Intra Cl(1)----O(1) interaction of complex **5**.

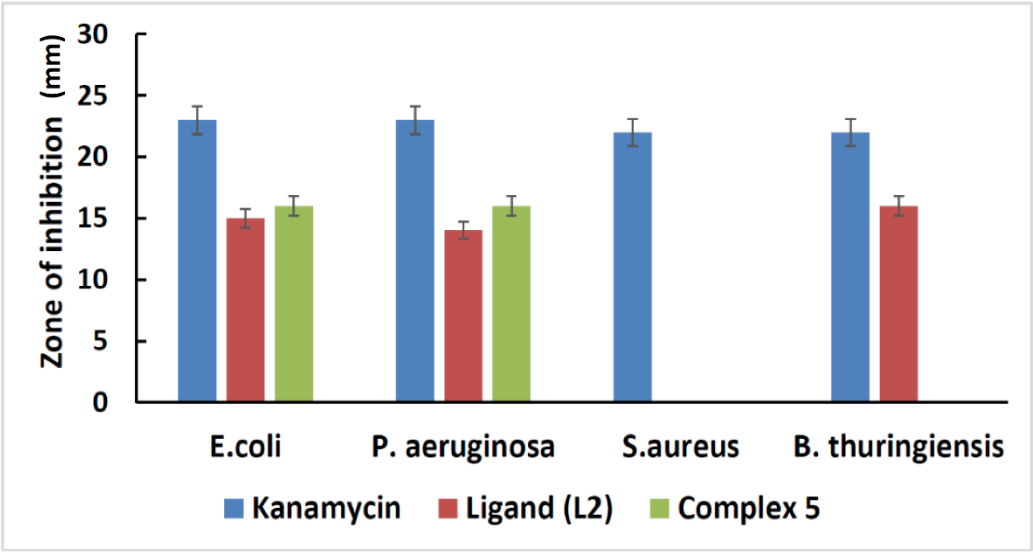

Figure 6: Antibacterial studies shown by ligand (**L2**) and complex **5** against Gram-positive and Gram-negative bacteria with kanamycin as the reference.

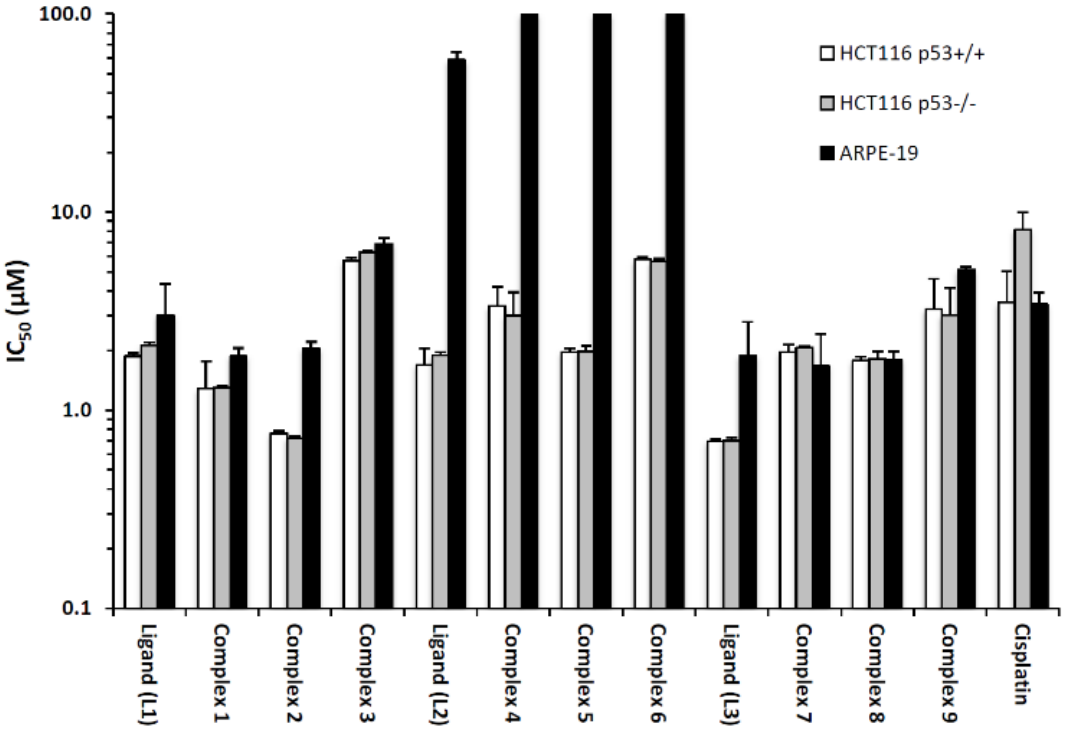

476

477 **Figure 7:** The response of cell lines following continuous 96-hour exposure to compounds. Each
478 value represents the mean IC_{50} value ± standard deviation for three independent experiments. *
479 denotes results where the IC_{50} is higher than the highest dose tested (100 μM). $^{+}$ denotes data
480 originally obtained and published.

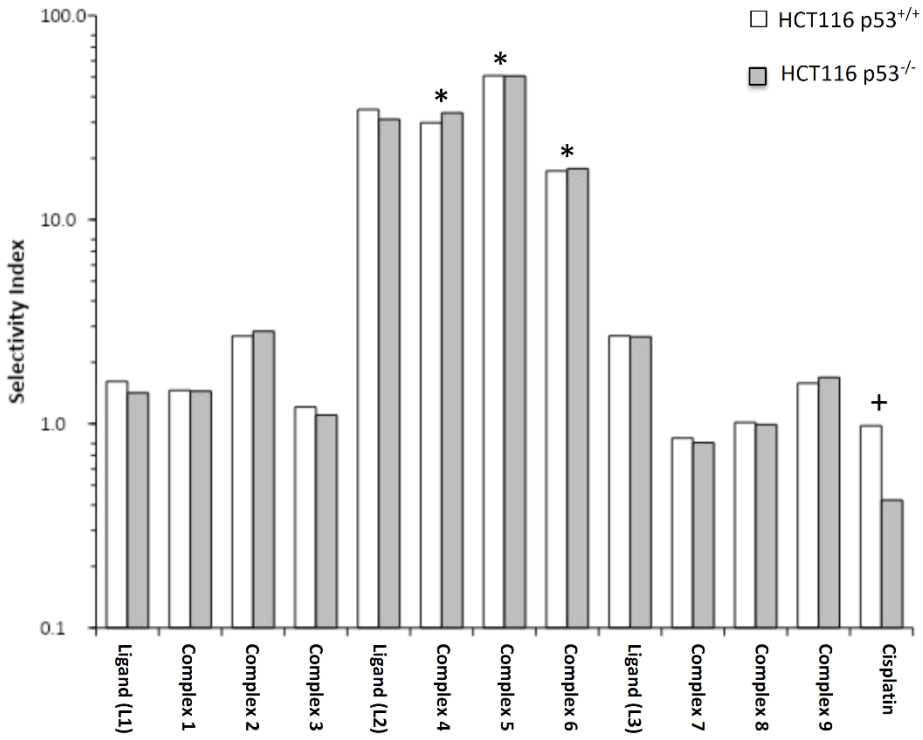

Figure 8: Selectivity indices for compounds and cisplatin.The selectivity index is defined as the ratio of IC_{50} values for ARPE-19 cells divided by the mean IC_{50} for HCT116 $p53^{+/+}$ and $p53^{-/-}$ cells (values > 1 indicate selectivity for cancer as opposed to non-cancer cells). As these parameters were calculated based upon the mean IC_{50} values, no error bars are presented here. *denotes results where the IC_{50} is higher than the highest dose tested (100 μM) and $^{+}$ denotes data derived from IC_{50} data originally obtained and published.

Table 1: Crystal structure data and refinement of complexes **1**, **2**, **3**, **4**, **5** and **7**

Complexes	[**1**]PF_6	[**2**]PF_6	[**3**]PF_6	[**4**]PF_6	[**5**] PF_6	[**7**]PF_6
Empirical formula	$C_{30}H_{31}ClF_6N_3O_2PRu$	$C_{30}H_{32}ClF_6N_3O_2PRh$	$C_{30}H_{32}ClF_6IrN_3O_2P$	$C_{29}H_{29}ClF_6N_3O_2PRu$	$C_{29}H_{30}ClF_6N_3O_2PRh$	$C_{29}H_{29}ClF_6N_3OPRu$
Formula weight	747.07	749.91	839.2	733.04	735.89	717.05
Temperature (K)	290(1)	292(2)	293(2)	293.(2)	292(2)	292(2)
Wavelength (Å)	0.71073	0.71073	0.71073	0.71073	0.71073	0.71073
Crystal system	triclinic	orthorhombic	Orthorhombic	monoclinic	orthorhombic	triclinic
Space group	$P\bar{1}$	*P c c n*	*P c c n*	*P c*	*P c a 21*	$P\bar{1}$
a (Å)/α (°)	9.8493(4)/84.837(4)	33.1104(15)/90	14.868(3)/90	15.7044(5)/90	26.4391(9)/90	9.6683(7)/111.086(7)
b (Å)/β (°)	11.0752(5)/73.502(4)	14.9267(12)/90	33.177(7)/90	16.5866(5)/96.864(3)	8.6951(3)/90	11.9591(8)/92.056(6)
c (Å)/γ (°)	16.2195(7)/68.010(4)	14.8349(9)/90	14.909(3)/90	11.8226(3)/90	26.7128(12)/90	14.0098(10)/97.881(6)
Volume ($Å^3$)	1572.75(13)	7331.8(8)	7354(3)	3057.51(16)	6141.0(4)	1490.76(19)
Z	2	8	8	4	8	2
Density (calc) (Mg/m^{-3})	1.578	1.359	1.516	1.592	1.592	1.597
Absorption coefficient	0.703	0.641	3.806	0.721	0.764	0.735
F(000)	756	3040	3296	1480	2976	724
Crystal size (mm^3)	0.21 x 0.19 x 0.15	0.30 x 0.20 x 0.15	0.29 x 0.23 x 0.16	0.29 x 0.23 x 0.16	0.23 x 0.12 x0.12	0.23 x 0.11 x 0.11
Theta range for data collection	3.9040 to 27.7150°	3.861 to 26.217	4.044 to 26.144°	3.5380 to 28.8130°	3.615 to 26.704°	3.7360 to 27.6580°
Index ranges	-13<=h<=13,-14<=k<=14, -21<=l<=21	-44<=h<=19,-20<=k<=8, -12<=l<=17	-11<=h<=18, -43<=k<=20, -20<=l<=9	-9<=h<=19, -20<=k<=22, -16<=l<=15	-34<=h<=28, -11<=k<=8, -33<=l<=27	-13<=h<=12, -15<=k<=14, -9<=l<19
Reflections collected	12338	15216	15603	11744	16131	10424
Independent reflections	7104 [R(int) = 0.0331]	7554 [R(int) = 0.0328]	7990 [R(int) = 0.0506]	8176 [R(int) = 0.0219]	10139 [R(int) = 0.0372]	6707 [R(int) = 0.0324]
Completeness to theta = 25.00°	99.81 %	91.9%	93.29%	98.89 %	99.03 %	99.13 %
Absorption correction	Semi-empirical from equivalents	Semi-empirical from equivalents	Semi-empirical from equivalents	Semi-empirical from equivalents	Semi-empirical from equivalents	Semi-empirical from equivalents
Refinement method	Full-matrix least-squares on F^2	Full-matrix least-squares on F^2	Full-matrix least-squares on F^2	Full-matrix least-squares on F^2	Full-matrix least-squares on F^2	Full-matrix least-squares on F2
Data/restraints/parameters	7104/0/397	7554/0/404	7990/1/404	8176/2/775	10139/229/834	6707/0/379
Goodness-of-fit on F_2	1.053	1.024	1.032	1.007	1.031	1.106
Final R indices [I>2sigma(I)]	R1 = 0.0487, wR2 = 0.0961	R1 = 0.0561, wR2 = 0.1400	R1 = 0.0558, wR2 = 0.1114	R1 = 0.0348, wR2 = 0.0787	R1 = 0.0584, wR2 = 0.1341	R1 = 0.0575, wR2 = 0.1484
R indices (all data)	R1 = 0.0626, wR2 = 0.1040	R1 = 0.0828, wR2 = 0.1579	R1 = 0.1035, wR2 = 0.1302	R1= 0.0424, wR2 = 0.083	R1 = 0.0828, wR2 = 0.1514	R1 = 0.0725, wR2 = 0.1604
Largest diff. peak and hole ($e.Å^{-3}$)	0.615 and -0.480	0.700 and -0.375	1.182 and -1.910	0.690 and -0.468	1.241 and -0.844	1.054 and -0.658
CCDC No.	1943881	-	1943880	1943884	1943882	1943883

Structures were refined on F_0^2: $wR_2 = [\Sigma[w(F_0^2 - F_c^2)^2] / \Sigma w(F_0^2)^2]^{1/2}$, where $w^{-1} = [\Sigma(F_0^2)+(aP)^2+bP]$ and $P = [\max(F_0^2, 0)+2F_c^2]/3$

Table 2: Selected bond lengths (Å) and bond angles (°) of complexes

Complexes	**1**	**2**	**3**	**4**	**5**	**7**
M(1)-CNT	1.6693(1)	1.7787(1)	1.7926(4)	1.670(3)	1.7841(1)	1.6646(1)
M(1)-N(1)	-----	2.087(4)	2.070(6)	-----	2.090(8)	-----
M(1)-N(2)	2.128(2)	2.110(3)	2.076(6)	2.136(4)	2.114(7)	2.144(3)
M(1)-O(1)	2.086(2)	-----	-----	2.077(4)	-----	2.097(3)
M(1)-Cl(1)	2.3853(10)	2.4035(12)	2.405(2)	2.4044(16)	2.418(3)	2.3852(11)
N(2)-M(1)-O(1)	76.35(9)	-----	-----	76.30(15)	-----	76.51(10)
N(2)-M(1)-Cl(1)	84.50(8)	86.76(10)	85.84(17)	84.27(13)	87.6(2)	84.40(8)
N(1)-M(1)-N(2)	-----	76.01(14)	75.6(2)	----	76.3 (3)	----
N(1)-M(1)-Cl(1)	-----	85.08(10)	83.93(17)	----	111.2(4)	----
O(1)-M(1)-Cl(1)	85.16(7)	-----	-----	84.53(12)	-----	84.71(8)

CNT represents the centroid of the arene/Cp* ring and (M = Ru, Rh and Ir).

Table 3: The response of cell lines following continuous 96-hour exposure to ligands, complexes and cisplatin. Each value represents the mean IC_{50} value ± standard deviation for three independent experiments

Compounds	IC_{50}(μM)		
	HCT116+/+	**HCT116 -/-**	**ARPE19**
Ligand (L1)	1.867± 0.083	2.124 ± 0.078	3.009 ± 1.341
Complex 1	1.282 ± 0.481	1.294 ± 0.038	1.869 ± 0.192
Complex 2	0.764 ± 0.02	0.723 ± 0.019	2.055 ± 0.156
Complex 3	5.704 ± 0.158	6.239 ± 0.088	6.887 ± 0.501
Ligand (L2)	1.690 ± 0.356	1.887 ± 0.068	58.544 ± 5.391
Complex 4	3.352 ± 0.839	2.998 ± 0.946	100.000 ± 0.000
Complex 5	1.970 ± 0.077	1.976 ± 0.134	100.000 ± 0.000
Complex 6	5.771 ± 0.161	5.621 ± 0.189	100.000 ± 0.000
Ligand (L3)	0.695 ± 0.017	0.703 ± 0.023	1.874 ± 0.915
Complex 7	1.969 ± 0.175	2.074 ± 0.035	1.676 ± 0.752
Complex 8	1.775 ± 0.087	1.818 ± 0.164	1.801 ± 0.172
Complex 9	3.228 ± 1.358	3.024 ± 1.109	5.100 ± 0.210
Cisplatin	3.51 ± 1.5	8.12 ± 1.83	3.43 ± 0.48

Table 4: Selectivity indices for ligands, complexes and cisplatin. The selectivity index is defined as the ratio of IC_{50} values for ARPE-19 cells divided by the mean IC_{50} for HCT116 $p53^{+/+}$ and $p53^{-/-}$ cells (values > 1 indicate selectivity for cancer as opposed to non-cancer cells)

Compounds	**HCT116+/+**	**HCT116 -/-**
Ligand (L1)	1.61	1.42
Complex 1	1.46	1.44
Complex 2	2.69	2.84
Complex 3	1.21	1.10
Ligand (L2)	34.64	31.02
Complex 4	29.83	33.36
Complex 5	50.76	50.61
Complex 6	17.33	17.79
Ligand (L3)	2.70	2.67
Complex 7	0.85	0.81
Complex 8	1.01	0.99
Complex 9	1.58	1.69
Cisplatin	0.98	0.42